International Journal of Biological Macromolecules 269 (2024) 131962

Contents lists available at ScienceDirect

International Journal of Biological Macromolecules

journal homepage: www.elsevier.com/locate/ijbiomac

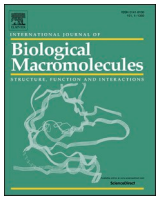

Magnetic carbon nanotubes modified with proteins and hydrophilic monomers: Cytocompatibility, *in-vitro* toxicity assays and permeation across biological interfaces

Mariana Azevedo Rosa [a], Andreia Granja [b], Cláudia Nunes [b], Salette Reis [b], Ana Beatriz Santos da Silva [c], Ketolly Natanne da Silva Leal [c], Marco Aurélio Zezzi Arruda [c], Luiz Fernando Gorup [d,e,f], Mariane Gonçalves Santos [a], Marcos Vinicios Salles Dias [g], Eduardo Costa Figueiredo [a,*]

[a] *Laboratory of Toxicant and Drug Analyses, Faculty of Pharmaceutical Sciences, Federal University of Alfenas, 37130-001 Alfenas, MG, Brazil*
[b] *LAQV, REQUIMTE, Department of Chemical Sciences, Faculty of Pharmacy, University of Porto, Rua Jorge de Viterbo Ferreira, 228, 4050-313 Porto, Portugal*
[c] *Spectrometry, Sample Preparation and Mechanization Group, Institute of Chemistry, University of Campinas – Unicamp, P.O. Box 6154, Campinas, SP 13083-970, Brazil*
[d] *Institute of Chemistry, Federal University of Alfenas, 37130-001 Alfenas, MG, Brazil*
[e] *School of Chemistry and Food Science, Federal University of Rio Grande, Av. Italia km 8 Bairro Carreiros, 96203-900 Rio Grande, RS, Brazil*
[f] *Materials Engineering, Federal University of Pelotas, Campus Porto, 96010-610 Pelotas, RS, Brazil*
[g] *Institute of Natural Sciences, Federal University of Alfenas, 37130-001 Alfenas, MG, Brazil*

ARTICLE INFO

Keywords:
Functionalized carbon nanotubes
Cytocompatibility
Caco-2 permeation

ABSTRACT

Carbon nanotubes are promising materials for biomedical applications like delivery systems and tissue scaffolds. In this paper, magnetic carbon nanotubes (M-CNTs) covered with bovine serum albumin (M-CNTs-BSA) or functionalized with hydrophilic monomers (M-CNTs-HL) were synthesized, characterized, and evaluated concerning their interaction with Caco-2 cells. There is no comparison between these two types of functionalization, and this study aimed to verify their influence on the material's interaction with the cells. Different concentrations of the nanotubes were applied to investigate cytotoxicity, cell metabolism, oxidative stress, apoptosis, and capability to cross biomimetic barriers. The materials showed cytocompatibility up to 100 μg mL^{-1} and a hemolysis rate below 2 %. Nanotubes' suspensions were allowed to permeate Caco-2 monolayers for up to 8 h under the effect of the magnetic field. Magnetic nanoparticles associated with the nanotubes allowed estimation of permeation through the monolayers, with values ranging from 0.50 to 7.19 and 0.27 to 9.30 × 10^{-3} μg (equivalent to 0.43 to 6.22 and 0.23 to 9.54 × 10^{-2} % of the initially estimated mass of magnetic nanoparticles) for cells exposed and non-exposed to the magnets, respectively. Together, these results support that the developed materials are promising for applications in biomedical and biotechnological fields.

1. Introduction

Due to their unique combination of chemical, physical, optical, and mechanical properties, carbon nanotubes (CNTs) are promising materials for a wide range of applications [1,2]. CNTs present a high surface area, the possibility to be functionalized, and the capacity to bind to organic molecules [1,2]. The use of CNTs in the biomedical and biotechnological fields involves tissue and cell imaging, tissue engineering, the development of biosensors, and applications in delivery systems (drugs, vaccines, genes, *etc.*) [3–9]. Concerns about nanotoxicity have increased in the last few years, and the use of nanomaterials in biomedical procedures is conditioned by their biocompatibility [9]. Therefore, during the development of a new material, *in vitro* assays are the first tests performed to ensure the continuity of the studies [8,9]. Tests that evaluate cytotoxicity, cell metabolism, oxidative stress, and morphological structures can be performed to infer

* Corresponding author at: Laboratory of Toxicant and Drug Analyses, Faculty of Pharmaceutical Sciences, Federal University of Alfenas, 37130-001 Alfenas, MG, Brazil.
E-mail address: eduardo.figueiredo@unifal-mg.edu.br (E.C. Figueiredo).

https://doi.org/10.1016/j.ijbiomac.2024.131962
Received 28 November 2023; Received in revised form 26 March 2024; Accepted 27 April 2024
Available online 29 April 2024

the material's cytocompatibility [10].

Modifications in CNTs provide a variety of functional groups for specific and selective conjugation. The functionalization might improve the dispersibility, cytocompatibility, and biodistribution of the materials, confer magnetics properties, and enhance the site-specific targeting [9]. Some authors reported that the functionalization or pre-incubation with proteins reduced the material cytotoxicity [11,12]. Long et al. (2018) concluded that pre-incubation with BSA increased the internalization of multi-walled CNTs in human umbilical vein endothelial cells (HUVECs). The better internalization reduced the cytotoxicity and the oxidative stress but enhanced the inflammatory response [11]. Lu et al. (2018) investigated the binding of human plasma proteins with carboxylate single-walled CNTs. The authors observed that adsorbed proteins influenced the cytotoxicity and neutrophil response caused by the nanomaterials [12]. Ding et al. (2017) demonstrated that single-walled CNTs covered with BSA had a higher degradation degree when compared to pristine CNTs in zymosan-stimulated macrophages. Additionally, the degradation of CNTs covered with BSA induced less cytotoxicity [13]. The literature reported that functionalization with other chemical groups also brings benefits to CNTs. For example, Zhou et al. (2017) demonstrated that CNTs functionalized with -OH and -COOH groups induced less cell death but led to more genotoxic effects compared to pristine CNTs [14]. Additionally, some authors demonstrated the advantages of using magnetic materials. Kaboudin et al. (2018) modified multi-walled CNTs with pyridine and magnetic nanoparticles. The material was used to transport nucleic acids through cell membranes, and an external magnetic field was applied to remove the nanocarriers from the cells [15]. Xu et al. (2018) used CNTs with paramagnetic cationic surfactants to obtain an endocytosis transfection platform, allowing the delivery of DNA and proteins [16]. As another example, Hu et al. (2019) developed a strategy to provide natural cell membranes-camouflaged magnetic CNTs using ephrinb2/HEK293 cells. The material was employed to screen drug leads targeting membrane receptors from traditional Chinese medicine, and presented suitable stability, binding capacity and selectivity [17].

The functionalization of the materials' surfaces might interfere with the capacity of CNTs to cross biological membranes. Gonzalez-Carter et al. (2019) observed that CNTs functionalized with polymers (M4VP, PGMA, or SPMAK) could penetrate cells by endocytosis mechanisms, and the permeation rates were dependent on the surface charge. Anionic CNTs were less toxic but had a lower permeation when compared to non-ionic and cationic ones [7]. However, the findings of Kostarelos et al. (2007) did not corroborate the previous work. The authors concluded that the uptake of CNT was independent of the functional group and cell type [18].

Human colorectal adenocarcinoma cells, namely Caco-2, are commonly used to cultivate biomimetic intestinal barriers due to their ability to differentiate and form a monolayer with characteristics like the enterocytes [19,20]. Thus, the absorption of nanomaterials after oral administration can be evaluated by permeation assays [21], bringing valuable data for developing delivery devices. Some papers evaluated the oral administration of carbon nanotubes. Kolosnjaj-Tabi et al. (2010) did not observe death or trouble in the growth or behavior of Swiss mice after oral administration of large doses of ultrashort and full-length single-walled carbon nanotubes [22]. Prajapati et al. (2012) demonstrated a linear relationship between the percentage of inhibition of Leishman and an oral dose of amino-functionalized CNTs containing amphotericin B. An oral administration of a 5-day course at 15 mg kg^{-1} body weight in the hamster model resulted in 99 % inhibition of parasite growth [23]. Chen et al. (2018) showed that low doses of CNTs did not lead to pathological damage in the duodenum or colon after oral administration. However, large concentrations could lead to injuries and changes in gut microbiota. The authors also observed that multi-walled CNTs caused a less severe impact on the intestinal tract than single-walled carbon nanotubes [24]. Finally, Espíndola et al. (2022) observed that CNTs were non-toxic for normal cell lines within a wide concentration range and that single-walled carbon nanotubes could be applied as nanocarriers for oral administration of 7-Hydroxyflavon [25].

Our research group recently proposed successful modifications of magnetic CNTs with BSA chemically crosslinked (M-CNTs-BSA) and CNTs with hydrophilic monomers (CNTs-HL) for sample preparation of biological matrices [25,26]. This study aims to evaluate whether these modified CNTs are also promising for biomedical applications. As mentioned above, there is no comparison between these two types of functionalization (protein and hydrophilic monomers) in literature, and this study can provide useful data for understanding the role of the surface in the interaction of material with cells. Therefore, the main aims of this work were deeply investigating the cytocompatibility of M-CNTs, M-CNTs-BSA, and M-CNTs-HL through different assays, comparing the strengths and weaknesses of each functionalization, and exploring the influence of an external magnetic field on the material's permeation in Caco-2 cells. These studies are important since CNTs have favorable characteristics for biomedical applications, but the biocompatibility of the pristine CNTs is still a limiting factor. In addition, a positive influence of the magnetic field on the material's permeation can be useful in further research and applications. Generally, the effects of CNTs in a cell's monolayers were only accessed by the measurement of the integrity of the barrier. However, our study allowed us to estimate the quantity of permeate materials due to the presence of magnetic nanoparticles. The application and comparison of these materials in the proposed paper are novel approaches that contribute to understanding the interactions of magnetic CNTs and their surface groups with biological systems.

2. Methods

2.1. Reagents and solution

Multi-walled CNTs (95.0 % purity, external wall diameters from 6 to 9 nm and lengths of 5 mm), BSA (96.0 % purity), sodium borohydride, iron (III) chloride hexahydrate, iron (II) sulfate heptahydrate, tetraethyl orthosilicate, 3-methacryloxypropyltrimethoxysilane, glycerol-dimethacrylate, 2-hydroxyethyl acrylate, methanol (HPLC grade), Triton X-100, trypan blue dye, and 2′,7′-dichlorofluorescein diacetate (DCFH-DA) were purchased from Sigma-Aldrich® (St. Missouri, USA). Ammonium hydroxide, ethanol, and isopropyl alcohol were supplied by Exodus Scientifica® (São Paulo, Brazil). Glutaraldehyde (50 % solution in water) and sodium borohydride were supplied by Dinâmica® (São Paulo, Brazil). A lactate dehydrogenase (LDH) detection kit and an Annexin V with the 7-aminoactinomicyn staining kit were obtained from Takara Bio Inc.®. (Shiga, Japan) and from Molecular Probes® (Eugene, USA), respectively. Hanks' Balanced Salt Solution [−] $CaCl_2$, [−] $MgCl_2$ (HBSS), Dulbecco's modified Eagle medium (DMEM), trypsin-EDTA, phosphate-buffered saline (PBS), resazurin, formalin, propidium iodide, penicillin-streptomycin, and fetal bovine serum were acquired from Gibco by Life Technologies® (Paisley, UK). Invitrogen™ Cell Mask™ and Hoechst 33342® dyes were purchased from ThermoFisher® (Agawam, USA). H_2O_2 30 % was obtained from Acros Organics® (Geel, Belgium). The ultra-high purity water (18.2 MΩ cm) had been previously purified in a Milli-Q® system (Millipore, Bedford, EUA). The Caco-2 cell line was acquired from the American Type Culture Collection (ATCC, Wesel, Germany), and the L929 cell line was purchased from Cell Lines Service (CLS, Eppelheim, Germany).

2.2. Syntheses

2.2.1. Magnetic carbon nanotubes

The magnetic materials were synthesized by modifications of previously described methods [26,27]. The synthesis occurred under an N_2 atmosphere and vigorous stirring. First, iron (III) chloride hexahydrate (428 mg) and iron (II) sulfate heptahydrate (627 mg) were dissolved in ultrapure water (50 mL) in a three-neck bottle flask. Subsequently, 250

mg of commercial CNTs (for M-CNTs as final material and M-CNTs-BSA) or previously oxidized CNTs (for M-CNTs-HL) were dispersed in the solution and stirred for 10 min. Finally, ammonium hydroxide (2.5 mL) was added dropwise to the synthesis medium, and the reaction occurred for 30 min. The obtained materials were washed with ultrapure water until the pH was neutral and then dried at 60 °C for 24 h. Fig. 1 schematizes the synthesis process for obtaining magnetic carbon nanotubes, as well as the procedures for functionalizing their surfaces.

2.2.2. Magnetic carbon nanotubes covered with albumin

The M-CNTs were encapsulated with BSA to obtain the M-CNTs-BSA, according to the procedure adapted from Mendes et al. (2020) [28]. A BSA solution (1 % v/v, prepared in a 50 mmol L^{-1}, pH 6.0 phosphate buffer) (20.0 mL) was added to a 50 mL glass flask containing M-CNTs (500 mg). The mixture was sonicated for 10 min and maintained on standby for another 10 min. Then, the material was separated using a magnet, and the supernatant was discarded. A 25 % (m/v) glutaraldehyde aqueous solution (5.0 mL) was added to the M-CNTs, and the flask was gently stirred for 5 h. After, the supernatant was discarded, and the material was dispersed in an aqueous borohydride solution (1 % m/v) (10.0 mL) under agitation for 15 min. The M-CNTs-BSA were separated, washed with ultrapure water (until no foam, typical of proteins, was observed in the supernatant), and dried (60 °C for 24 h).

2.2.3. Magnetic carbon nanotubes functionalized with hydrophilic monomers

The synthesis of M-CNTs-HL was performed similar to the method developed by De Faria et al. (2022) [29]. First, commercial CNTs (500 mg) were oxidized by 65 % (m/m) nitric acid (60.0 mL) under reflux at 120 °C for 90 min. After this step, the resulting material was cooled to room temperature, thoroughly washed with ultrapure water until reaching a neutral pH (using a vacuum filtration system), and then dried at 60 °C for 24 h. The oxidized CNTs were magnetized according to the method described above (2.2.1). Then, the oxidized M-CNTs (300 mg) were dispersed in isopropyl alcohol:water (5:1, v:v) (30.0 mL). Ammonium hydroxide 28 % (m/m) (10.0 mL) and tetraethyl orthosilicate (TEOS) (4.0 mL) were added to the mixture, which remained in constant stirring for 12 h at room temperature. The obtained M-CNTs-TEOS were washed with ultrapure water until the white supernatant from the first washes (TEOS remnants) was replaced by a clear supernatant and dried as previously described. In the next step, 3-methacryloxypropyltrimethoxysilane (MPS) (4.5 mL) was added dropwise (under an ultrasonic bath) into a glass flask containing the intermediate material (300 mg) and methanol (50.0 mL). The synthesis occurred under stirring for 48 h at room temperature. The obtained material (M-CNT-TEOS-MPS) was rinsed with methanol to remove the excess reagents and dried. Next, glycerol dimethacrylate, GDMA, (0.225 mL) and 2-hydroxyethyl acrylate, HEA, (2.1 mL) were added to a suspension comprising the MPS-functionalized material (200 mg) in methanol (30.0 mL). The reaction was maintained at room temperature with stirring for 24 h. Finally, the M-CNTs-HL were washed with methanol and dried at 60 °C for 24 h.

2.3. Characterization

Surface area and porosity analyses were performed using a Gemini VII 3.03 (Micromeritics Instrument Corporation, Norcross, USA), operating with an equilibrium time of 5 s, and using nitrogen as sorbent gas. BET (Brunauer-Emmett-Teller) method was used to calculate the surface area, while the BJH (Barrett-Joyner-Halenda) method was used to obtain the pore volume.

A Zeiss Supra 35VP field effect electron gun (FEG-SEM) microscope, operating at 10 keV and spot 3 was employed to verify the size and morphology of the samples. To prepare the samples, small fragments of materials were placed on a silicon substrate secured with carbon tape. Finally, the samples were oven-dried at 40 °C for 12 h. Analysis using a 2D energy dispersive X-ray detector (EDS) was performed with 2D mapping at 25 keV and spot 4. The 2D EDS images were generated based on the energy released from the emission of C Kα, O Kα, and Fe Lα1.

Fourier transform infrared spectroscopy (FTIR) analyses were conducted with an Affinity-1 (Shimadzu®, Japan) spectrophotometer and potassium bromide pastilles. The spectra were recorded in transmittance mode (4000–400 cm^{-1}) at room temperature, using 34 scans per analysis at a resolution of 4.0 cm^{-1}. A blank potassium bromide pastille was used to correct the background. Additionally, the obtained spectra were treated with OriginLab® software.

Laser doppler velocimetry (Zetasizer ZS Nano, Malvern Penalytical®, Malvern, UK), with a detection angle of 173° and operating at 25 °C, was used to evaluate the zeta potential. Nine suspensions (150 μg mL^{-1}) of the synthesized materials were prepared in ultrapure water with pH adjusted from 2.0 to 10.0. The suspensions were left on standby for 3 h

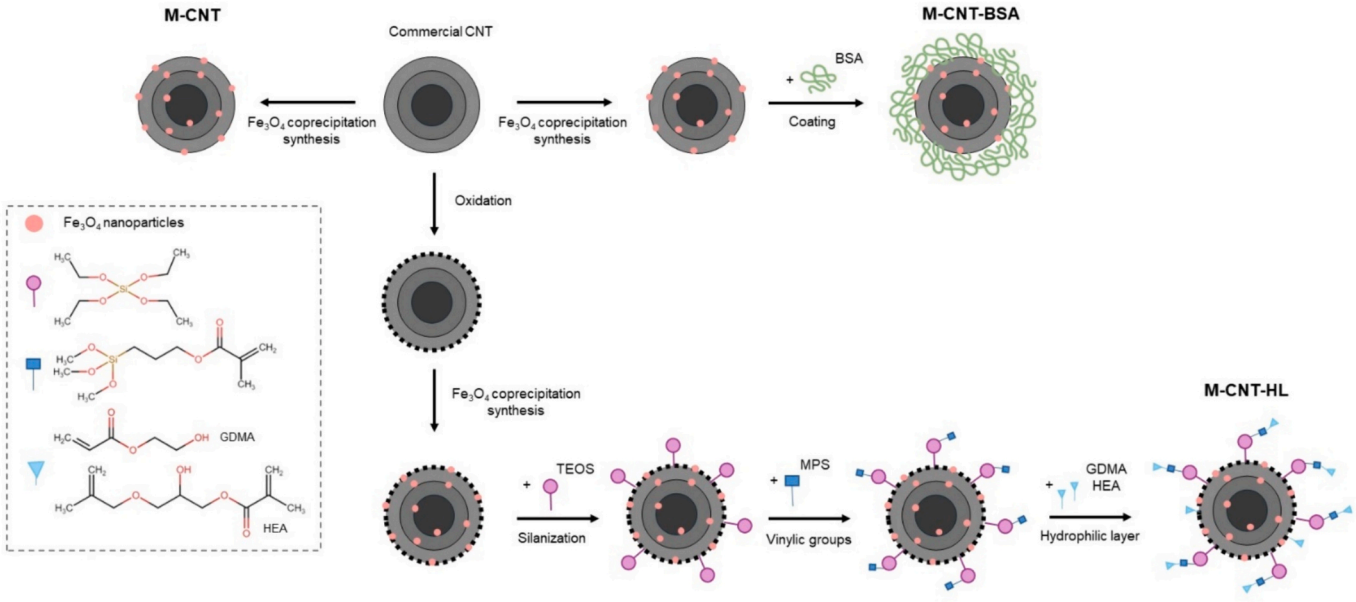

Fig. 1. Synthesis scheme for obtaining M-CNT, M-CNT-BSA, and M-CNT-HL. Note: TEOS: tetraethyl orthosilicate, MPS: 3-methacryloxypropyltrimethoxysilane, HEA: 2-hydroxyethyl acrylate, GDMA: glycerol dimethacrylate.

before the measurements ($n = 3$).

An SDT Q600 (TA Instruments®, New Castle, EUA) was used to perform the thermogravimetric (TGA) analyses. The atmosphere was composed of nitrogen (100 L min^{-1}) and the temperature ranged from 30 to 900 °C (heating rate of 20 °C min^{-1}).

For the X-ray analyses, a Rigaku (Ultima IV, Tokyo, Japan®) diffractometer with CuKα, α = 1.54051 Å, was employed. The 2θ scan interval was from 10 to 80°, with an angular step of 4° min^{-1}; the current was set to 30 mA, and the voltage was 40 kV.

The magnetic properties of M-CNT, M-CNT-BSA, and M-CNT-HL were measured using a SQUID-VSM (Quantum Design MPMS®3, San Diego, USA) at 300 K and under magnetic fields up to 2000 Oe.

Raman measurements were carried out at room temperature using a modular spectrometer setup comprising an Olympus B-X41 microscope and a Horiba iHR550 monochromator in backscattered photon detection geometry. The excitation source was a BWTek solid-state laser at 532 nm.

2.4. Albumin exclusion

Initially, a 50 mg L^{-1} BSA solution was prepared in phosphate buffer (10 mmol L^{-1}, pH 7.2). Next, a BSA solution (0.2 mL) was placed in test tubes with Bradford reagent (2.8 mL). After 10 min, the absorbance obtained was considered 100 % BSA. In the next step, 1 mL of the same BSA solution was added to test tubes containing 5 mg of each material (M-CNT, M-CNT-BSA, M-CNT-HL, $n = 3$). The tubes were shaken for 10 min. Afterward, the material was separated using a neodymium magnet, and an aliquot of the supernatant (0.2 mL) was treated with Bradford reagent as described above. The absorbance of the extracted BSA solution divided by the absorbance of the non-extracted BSA solution corresponded to the percent of protein excluded by the materials. The measurements were made in a KASUAKI (Model IL-593-BI) spectrophotometer operating at 595 nm.

2.5. Hemolysis assay

The hemoglobin release assay was performed according to Granja et al. (2021) [30]. Human blood samples were donated by Serviço de Hematologia from Centro Hospitalar Universitario do Porto - Hospital de Santo Antonio and collected from healthy donors in EDTA-coated tubes. First, the samples were centrifuged for 5 min (955 *g*, 4 °C). Then, the red blood cells (RBCs) were washed 3 times and diluted to a 4 % (v/v) solution with saline solution (0.85 %). The materials were suspended in saline solutions at concentrations of 500, 400, 250, 100, 50, and 25 μg mL^{-1} for M-CNTs and M-CNTs-HL and 100, 50, and 25 μg mL^{-1} for M-CNTs-BSA. Triton X-100 (1 % v/v) and saline solution were used as hemoglobin release positive and negative controls, respectively. Finally, 100 μL of RBCs were incubated (37 °C) with the materials suspension (100 μL) in a 96-well plate. After 1 h, the supernatant was removed, the absorbance of hemoglobin was measured at 415 nm using a microplate reader (Synergy™ HT Multi-mode, BioTek Instruments Inc.®, Winooski, VT, USA), and the percentage of hemolysis was calculated.

2.6. Cytocompatibility assays

Caco-2 and L929 cells lines were cultured in 75 cm^2 flasks with 10 mL of DMEM medium supplemented with 10 % (v/v) fetal bovine serum and 1 % (v/v) penicillin-streptomycin (37 °C, 5 % CO_2 atmosphere). Cells were supplied with fresh medium every 2–3 days and subcultured by chemical detachment with trypsin- EDTA when they reached 80–90 % confluency. Cell counting was performed in a Neubauer chamber after the addition of 25 % (v/v) trypan blue solution (0.4 %, w/v).

For resazurin and LDH assays, Caco-2 and L929 cells were seeded at a density of 5×10^4 cells per well in 96-well plates (100 μL per well) and cultured as described above. After 24 h, the culture medium was removed and replaced by different concentrations of each material suspension (100 μL): 500, 400, 250, 100, 50, and 25 μg mL^{-1} for M-CNT and M-CNT-HL, and 100, 50, and 25 μg mL^{-1} for M-CNT-BSA, prepared in supplemented DMEM medium. One mg mL^{-1} M-CNT, M-CNT-HL, and M-CNT-BSA suspensions, prepared in supplemented DMEM, were used for the dilutions after being sonicated for 3 min (using an ultrasonic bath). All samples were vortexed before their use.

After 24 h of incubation the plates were centrifuged (250 *g*, 10 min), and the supernatants were transferred to another 96-well plate to perform the LDH assay, according to the manufactures' manual (Takara Bio Inc.®, Shiga, Japan). Absorbances were then measured at 490 and 690 nm. Cytotoxicity was expressed as a percentage compared to the maximum cytotoxicity of Triton X-100 (1 % v/v). In turn, the attached cells were incubated with fresh culture medium containing resazurin (10 μg mL^{-1} for Caco-2 and 5 μg mL^{-1} for L929) for 4 h, and the fluorescence of resorufin (λex = 560 nm; λem = 590 nm) was measured using a microplate reader. DMEM and Triton-X 100 solution (1 % v/v) were used as controls for both assays.

The oxidative stress was evaluated by measuring the presence of intracellular reactive oxygen species, ROS, (mainly $OH^{\bullet}$) in Caco-2 cells after their exposure to the M-CNTs, M-CNTs-BSA, or M-CNTs-HL. Laser confocal microscopy and flow cytometry were employed to verify and quantify the presence of ROS in the cells. Supplemented DMEM medium and H_2O_2 solution (1 mmol L^{-1}, prepared in phosphate buffer saline - PBS) were used as negative and positive controls, respectively.

For the confocal microscopy analysis, Caco-2 cells (1×10^5 cells per well) were seeded on an 8-well μ-slide (Ibidi GmgH, Munich, Germany). After 24 h of incubation, the medium was replaced with 200 μL of M-CNTs, M-CNTs-BSA, or M-CNTs-HL suspensions (50 μg mL^{-1}). After 24 h, the supernatant of the positive control was removed, and H_2O_2 (1 mmol L^{-1}) was added and incubated for 1 h at room temperature. In the next steps, the media and materials' suspensions were removed, and cells were washed with PBS, followed by the addition of DCFH-DA (10 μmol L^{-1}, stock solution prepared in dimethyl sulfoxide and working concentration diluted in PBS) and incubation for 30 min. Finally, the cells were washed with PBS and stained with Invitrogen™ Cell Mask™ 0.1 % (incubated for 10 min in the dark), formalin solution (incubated for 30 min), and Hoechst 33342® (incubated for 10 min in the dark). The cells were washed with PBS after each step. A Leica Stellaris 8 (Leica Microsystems®, Wetzlar, Germany) laser confocal microscope was used for visualization using a $\lambda_{ex}/\lambda_{em}$ of 405/420–480 nm (Hoechst 33342®), 506/570–600 (DCFH-DA), and 649/690–750 nm (Cellmask™ Deep red). The data were acquired using the Leica Application Suite X package – LAS X software.

For the flow cytometry studies, Caco-2 cells were seeded in a 24-well plate (2×10^5 cells per well) and grown for 24 h. After this period, the cells were treated with 300 μL of materials suspensions (50 and 100 μg $mL^{-}1$) or H_2O_2 (1 mmol L^{-1}), as described previously. Afterward, the cells were detached with 0.5 % trypsin-EDTA, centrifuged (300 *g*, 5 min), resuspended in PBS, and stained with trypan blue (0.004 %) and propidium iodide dye (0.01 mg mL^{-1}). Finally, the cells were gently homogenized before analysis on a BD Accuri C6 (BD Biosciences®, Erembodegem, Belgium). For each sample, a minimum of 10,000 events were recorded.

The apoptosis assays were also performed using flow cytometry. Therefore, the Caco-2 cell seeding, exposure to the materials, and trypsinization occurred as described above. After the centrifugation, the cells were washed with cold PBS and centrifuged (300 *g*, 5 min). Next, the pellet was resuspended in cold PBS, the samples were treated with FITC Annexin V and 7-Amino-Actinomycin-D (7-AAD) staining kit (Biolegend®, California, USA), according to the manufacturer's manual, and analyzed using the BD Accuri C6 flow cytometer with a minimum of 10,000 events collected for each sample.

2.7. Caco-2 cells permeability assay

The permeability assay was performed similar to the method of

Granja et al. (2019) [20]. Caco-2 cells were seeded on a 12-well transwell device (polycarbonate membrane with pore diameter of 0.4 μm, Corning Incorporated, Corning, NY, USA) at a density of 1.12×10^5 cells per insert. Every 3–4 days, the cells received a fresh medium, and the integrity of the monolayer was monitored by measuring the transepithelial electrical resistance (TEER) with an epithelial voltohmmeter (EVOM) from World Precision Instruments (Sarasota, FL, USA).

After 21 days, the medium of Caco-2 monolayers was removed, and the cells were washed twice with HBBS buffer. M-CNTs, M-CNTs-BSA, and M-CNTs-HL suspensions (50 μg mL^{-1}, prepared in HBBS) were sonicated for 3 min (using an ultrasound bath) and vortexed before use. The experiments were conducted with transwell devices exposed and non-exposed to an external magnetic field (using neodymium magnets N52, 40 × 20 × 10 mm, 3700 G). Aliquots (0.3 mL) were taken from the basolateral side of the devices after 1, 4, 6, and 8 h. The samples were stored (−20 °C) for further analysis. Aliquots were also taken after 24 h of assay from the transwell device that was not exposed to the magnets. TEERs were measured at every aliquot withdrawal.

At the end of the permeation assays, the transwells were washed three times with PBS, and the monolayers were fixed and dyed, as described in Section 2.6. The membranes were removed from the inserts and placed in a glass slip (using Vectashield®) with a coverslip. The monolayers were then analyzed using confocal laser microscopy, using a $\lambda_{ex}/\lambda_{em}$ of 405/420–480 nm (Hoechst 33342®) and 649/690–750 nm (Cellmask™ Deep red) to stain cell nuclei and membranes, respectively.

The ^{57}Fe ions (from the magnetic nanoparticles) were used to estimate the concentrations of the nanotubes that permeated the Caco-2 barrier. First, the aliquots from the basolateral chamber were treated with nitric acid (0.1 mL). Samples were decomposed using an ultrasonic sonicator device with a cup-horn-shaped sonotrode (Qsonica®, Newtown, USA) at room temperature for 8 min (amplitude, 75 %; power, 210 W; energy, 4.087 J; pulse-on and pulse-off time, 1 min) [31]. Then, the extracted samples were diluted with ultrapure water to a final volume of 5.0 mL. The samples were analyzed by inductively coupled plasma mass spectrometry (ICP-MS, iCAP TQ, Thermo Scientific, Bremen, Germany). ^{57}Fe ions were quantified from a calibration curve (0.1–10 μg L^{-1}).

2.8. Statistical analysis

Statistical analyses were performed using R® software 4.2.1 (R Core Team, 2022). The difference among three or more groups was analyzed through ANOVA and Scott-Knott tests (for parametric statistics) or Kruskal-Wallis and Dunn (for non-parametric statistics). The tests were performed using a 0.05 significance level.

3. Results and discussion

3.1. Synthesis and characterization

M-CNTs, M-CNTs-BSA, and M-CNTs-HL were successfully synthesized. The Fe_3O_4 nanoparticles were deposited by chemical coprecipitation of iron (II) and iron (III) in the presence of pure or oxidized CNTs. The protein external layer in the surface of M-CNTs was formed by crosslinking the terminal amino groups of BSA molecules, using glutaraldehyde as a reagent. This process resulted in voluminous BSA-linked molecules bound by imine groups, which were converted to amino groups using sodium borohydride as a reducing agent [32–34]. The BSA layer was formed like a capsule on the outside of the material and did not build any covalent bonds with the nanotubes [34,35]. In its turn, the functionalization with the hydrophilic layer was obtained after different synthesis steps. Initially, pure CNTs were oxidized to promote a better interaction of the nanotubes with the reagents employed in the M-CNT-HL syntheses steps [36]. The oxidized CNTs were used to obtain magnetic materials, that were covalently functionalized with TEOS, MPS, and hydrophilic monomers (GDMA and HEA), promoting an external layer rich in -OH groups [29].

Commercial CNTs exhibited a BET surface area of 27.5342 $m^2\ g^{-1}$ and a pore volume of 0.008158 $cm^3\ g^{-1}$. M-CNTs displayed a higher surface area of 38.7388 $m^2\ g^{-1}$, probably due to the incorporation of the magnetic nanoparticles. Surface-functionalized materials, M-CNTs-BSA and M-CNTs-HL, showed lower BET surfaces of 24.0427 and 26.6449 $m^2\ g^{-1}$, respectively. The reduced surface area of these materials may be correlated to the presence of the external layers. Additionally, the slight increase in pore volume of M-CNTs-HL (0.018291 $cm^3\ g^{-1}$), compared to M-CNTs-BSA (0.011499 $cm^3\ g^{-1}$) and M-CNTs (0.013834 $cm^3\ g^{-1}$) could be due to the presence of the TEOS layer [37] . Supporting Table 1 summarizes these data.

The final materials, as well as their intermediate steps were characterized by different techniques. Morphological and structural aspects were evaluated by SEM. The analysis of Fe_3O_4 nanoparticles (Fig. 2a) showed that individual sizes were smaller than 50 nm, but they presented the tendency to form clusters larger than 1 μm. Fig. 2b-d and Fig. S1 refers to SEM images of pure CNTs at different magnitudes, showing a rough surface.

The SEM images demonstrated the homogeneous distribution of magnetite nanoparticles in carbon nanotubes in the M-CNTs-TEOS, M-CNTs-TEOS-MPS, M-CNTs-HL, M-CNTs, and M-CNT-BSA nanomaterials (Fig. 2e-i and Figs. S2-S11), suggesting that the particles were properly dispersed in the material without excessive concentration in specific areas of the nanotubes. Energy dispersive X-ray spectroscopy (EDS)

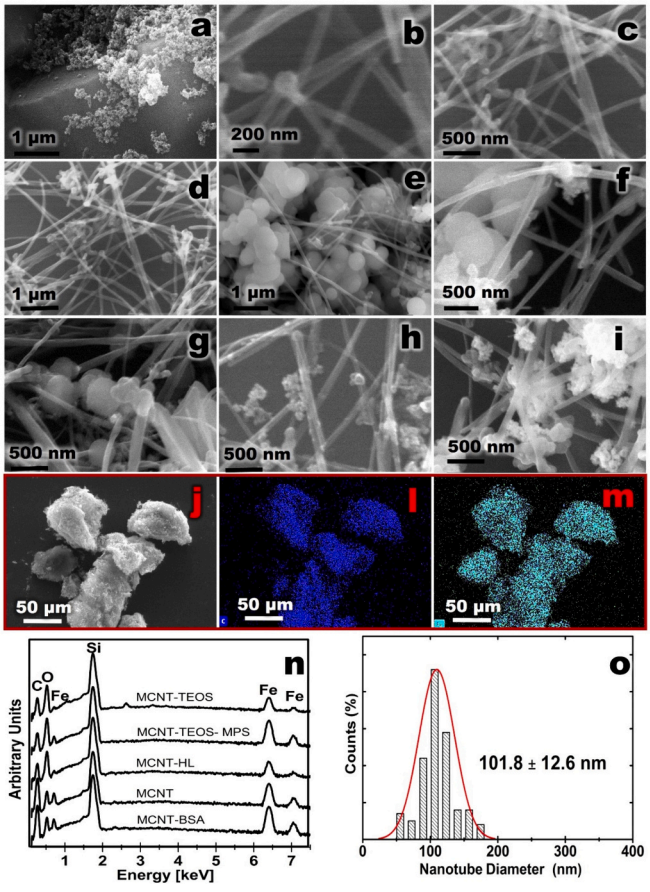

Fig. 2. SEM images of the synthesized materials (a) Magnetite nanoparticles Fe_3O_4; (b-d) pure CNTs at different magnitudes, (e) M-CNT-TEOS; (f) M-CNT-TEOS- MPS; (g) M-CNT- HL; (h) M-CNT; (i) M-CNT-BSA; (j-m) EDS elemental mapping of C Kα and Fe Kα of M-CNT-BSA. (n) EDS spectrum showing the presence of Fe, O, and C elements in all magnetic samples; (o) histogram fitted with a log-normal distribution of carbon nanotube diameter in the M-CNT-BSA sample.

could identify the presence of specific chemical elements, such as carbon, iron, and oxygen, and provided information about their distribution in the material [38]. The EDS analyses (Fig. 2j-m) of the composites reveal the presence of iron (Fe) from magnetite nanoparticles (turquoise spots) as well as carbon (C) from carbon nanotubes (blue shades). The 2D images were generated by analyzing the energy released from C Kα emissions from carbon nanotubes (Fig. 2l), as well as Fe Kα (Fig. 2m), indicating the uniform distribution of these elements in the demarcated area in the micrograph. SEM images were unable to distinguish magnetite particle sizes due to their proximity, but the EDS spectrum analysis made it possible to confirm the presence of iron oxide in the magnetic carbon nanotube composites. The EDS spectra of all magnetic samples are presented in Fig. 2n. The materials exhibited similar compositions, with emissions from C, O, and Fe atoms. In the region between 0.2 and 1.0 KeV, peaks corresponding to C Kα, O Kα, and Fe Lα emissions were clearly observed at 0.277, 0.525, and 0.705 keV, respectively. In the region between 6.0 and 7.0 keV, a peak at 6.398 keV corresponding to Fe Kα emissions was visible. The graph indicated the presence of carbon nanotubes and iron oxide nanoparticles and demonstrated the occurrence of C, O, and Fe atom in all the magnetic materials. Additionally, the EDS spectrum of the composite reveals the presence of Si elements (1.74 keV) originating from the silicon substrate used for sample deposition, as well as from the TEOS incorporation in M-CNT-TEOS, M-CNT-TEOS- MPS, and M-CNT- HL. Finally, the histogram of the SEM image indicated a carbon nanotube diameter of 101.8 nm (Fig. 2o).

Fig. 3a shows the FTIR spectra of M-CNT, M-CNT-BSA, M-CNT-HL, and their intermediated steps. The high absorption radiation by the black CNTs and their high symmetry resulted in spectra with low intensity. Bands around 2900 cm^{-1} could be related to stretching vibration C—H bounds of the pure and modified CNTs. The band at 580 cm^{-1}, presented in all the magnetic materials, could be referred to the iron of the Fe_3O_4 nanoparticles. Subtle bands at 1200 cm^{-1} and 1550 cm^{-1} might be related to the amine groups in the BSA layer presented in the M-CNT-BSA. Materials with TEOS showed bands that could be due to the

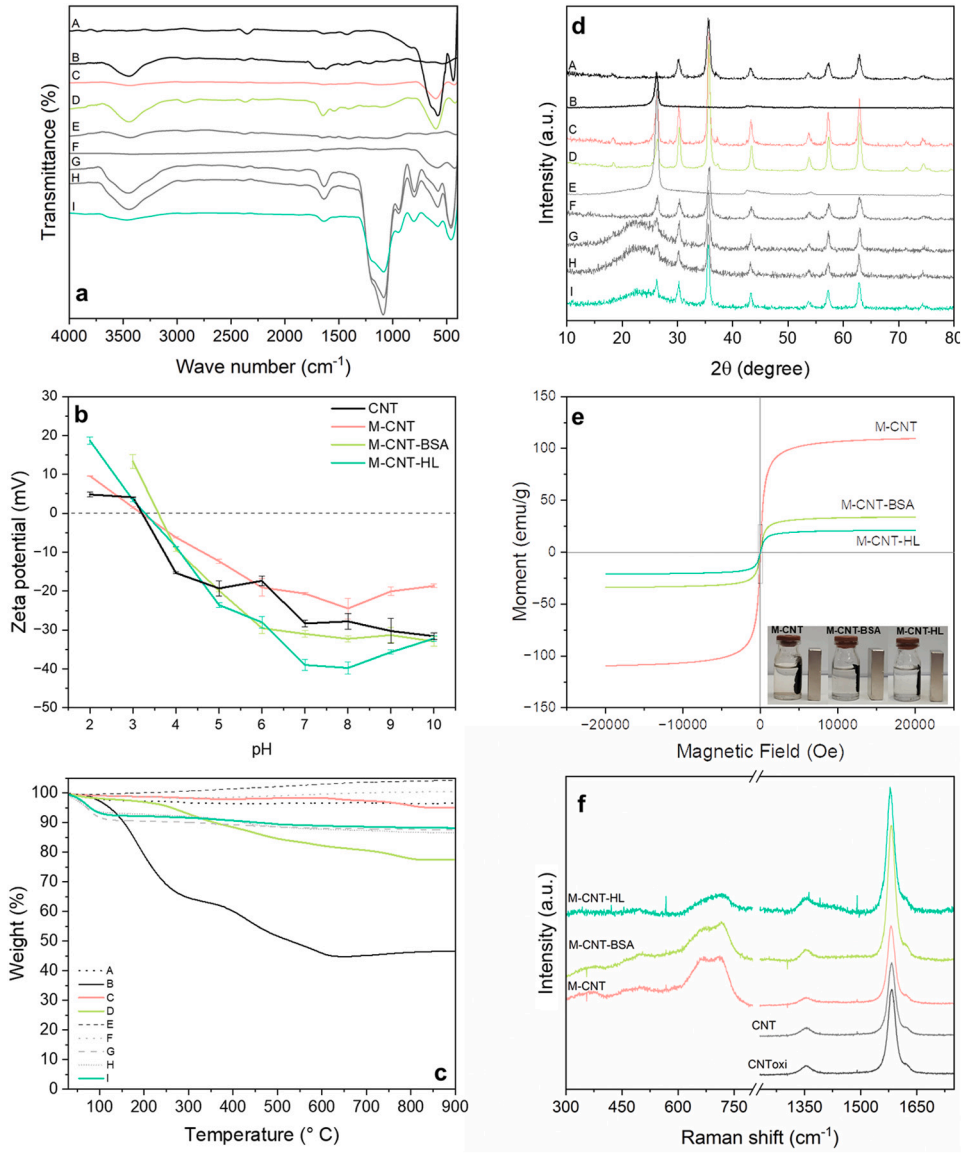

Fig. 3. Characterization of the synthesized materials. (a) Infrared spectroscopy. (b) Zeta potential analyses. (c) Thermogravimetric analyses. (d) X-ray patterns. (e) Magnetic hysteresis loop recorded at 300 K and photographs of M-CNT, M-CNT-BSA, and M-CNT-HL in the presence of a magnet. (f) Raman spectra for CNT, oxidized CNT, M-CNT, M-CNT-BSA, and M-CNT-HL. Note: When applicable, A: Fe_3O_4 nanoparticles; B: pure carbon nanotubes (CNT); C: magnetic carbon nanotubes (M-CNT); D: magnetic carbon nanotubes covered with bovine serum albumin (M-CNT-BSA); E-H: intermediate steps of M-CNT-HL, oxidized carbon nanotubes (CNToxi), magnetic oxidized carbon nanotubes, functionalization with TEOS, and functionalization with MPS; I: magnetic carbon nanotubes functionalized with the hydrophilic layer (M-CNT-HL).

interactions of Si-O-Si (1070 cm^{-1}), Si-O-H (952 cm^{-1}) and Si—O (815 and 476 cm^{-1}). Furthermore, the bands at approximately 3500 cm^{-1} may be due to O—H stretching of water vapor absorbed by the nanotubes. These bands may also be overlapped on the hydroxyl groups of hydrophilic monomers (in the case of M-CNT-HL) or N—H stretching, resulting from the functionalization with BSA.

The zeta potential analyses (Fig. 3b) showed that at pH 7.0 (near to the physiological pH) pure CNT, M-CNT, M-CNT-BSA, and M-CNT-HL have negatively charged surfaces (-28.33 ± 0.81, -36.6 ± 1.55, -31.00 ± 0.87, and -39.00 ± 1.35, respectively). The isoelectric points of these materials were estimated at 3.23 (CNT), 3.20 (M-CNT), 3.62 (M-CNT-BSA), and 3.28 (M-CNT-HL). Supporting Table 2 summarizes the zeta potential and isoelectric point of the final materials as well as their intermediate steps.

Thermal analyses are shown in Fig. 3c. Commercial CNTs exhibited a mass loss of approximately 55 % in temperatures above 570 °C. In contrast, the magnetic materials showed significantly lower mass loss, possibly due to the incorporation of the nanoparticles that remained stable up to temperatures higher than 900 °C. The M-CNTs lost about 5 % of their initial mass, while the M-CNTs-BSA lost approximately 33 % in two different events (the first probably related to BSA denaturation and degradation). The M-CNTs-HL lost around 12 % of the initial mass, possibly due to the scission of Si—O bonds arising from TEOS (their intermediate steps, M-CNTs-TEOS and M-CNTs-TEOS-MPS, exhibited similar profiles to M-CNTs-HL).

The diffractograms of the synthesized materials are shown in Fig. 3d. The peak at 26° can be correlated with the multi-welled CNT's diffraction pattern [39], whereas the peaks at 30°, 35°, 43°, 53°, 57°, and 62° can refer to the single cubic spinel-type crystalline phase of the magnetic nanoparticles [40]. The presence of these peaks in the samples is evidence of the nanoparticles' incorporation. Additionally, due to its amorphous characteristic, the BSA was not identified in the M-CNT-BSA diffractogram.

The saturation magnetization values for M-CNT, M-CNT-BSA, and M-CNT-HL (Fig. 3e) were 109.5, 33.9, and 21.0 emu g^{-1}, respectively. The decrease in these values from functionalized magnetic nanotubes can be attributed to the presence of non-magnetic amorphous groups in these materials [41,42]. However, despite the lower magnetic susceptibility, both M-CNT-BSA and M-CNT-HL demonstrated remarkable magnetic properties, enabling their recovery from solutions using a magnet (Fig. 3e). Additionally, the small hysteresis loops indicated that all analyzed materials exhibited paramagnetic behavior [41].

The Raman spectra (Fig. 3f) of all analyzed materials, including pure CNTs, oxidized CNTs, M-CNTs, M-CNTs-BSA, and M-CNTs-HL, exhibited two characteristic bands of multiwalled carbon nanotubes: the D band at 1340 cm^{-1} and the G band at 1570 cm^{-1}. The D band can result from sp^3 hybridized carbons or a disordered structure, while the G band stems from the splitting of the E_{2g} stretching mode of graphite [43]. The ratio of the D band area to the G band area was used to characterize the defects introduced during the oxidation of commercial CNTs. The D/G values of oxidized CNTs (0.125), which showed a higher D band, were higher than the D/G values of pure CNTs (0.114). The D/G value for M-CNTs-HL was 0.111, possibly indicating defect suppression by the functionalization with nanoparticles and TEOS. M-CNT and M-CNT-BSA presented D/G values of 0.100 and 0.101, respectively. Additionally, all magnetic materials exhibited a band at around 730 cm^{-1}, attributed to the magnetic nanoparticles [44].

3.2. Protein exclusion

M-CNT was able to exclude 48.72 ± 4.39 % of the protein molecules present in the BSA solution. The M-CNT-BSA and M-CNT-HL excluded 97.45 ± 1.88 and 79.92 ± 1.80 %, respectively (Fig. S12). The functionalization with BSA forms a voluminous external layer, hampering protein accumulation on the material's surface. Additionally, at pH values different from the isoelectric point of the proteins, electrostatic repulsion occurs between the layer of BSA and the BSA presented in the solution. The functionalization with GDMA and HEA created a dense and hydrophilic external layer, making the adsorption and the accumulation of proteins on the material's surface unfavorable [29,45].

When used in biomedical applications, the materials reach the bloodstream and interact with different proteins. According to the surface of the materials, the proteins can be adsorbed and accumulated, forming a protein corona which leads to some limitations. For examples, the size of the materials is increased (making them more likely to be recognized by the immune system), and the corona can lead to hemolysis and endothelial cell injury and cause undesirable internalizations [46,47]. Therefore, higher protein exclusion can be beneficial for using nanomaterials for biomedical applications.

3.3. Hemolysis and cytocompatibility assays

3.3.1. Hemolysis, resazurin, and lactate dehydrogenase release assays

An ultrasonic bath was used to improve the dispersibility of the nanotubes in the saline solution or DMEM. However, sedimentation occurred at around 20 min for M-CNT-BSA at concentrations of 500 and 400 μg mL^{-1}, probably due to the change in the density of the material with the BSA layer. Therefore, the highest concentration studied for this material was 100 μg mL^{-1}. These results agreed with the literature, as several studies that evaluated the cytocompatibility of CNTs functionalized with proteins used concentrations below 100 μg mL^{-1} [11,12,14]. Furthermore, it should be noted that only the final magnetic materials (M-CNT, M-CNT-BSA, and M-CNT-HL) were used in the *in vitro* assays once one of the main objectives of this work was to investigate the influence of an external magnetic field on the permeation of magnetic nanotubes across the biomimetic barrier. Additionally, previous studies observed no cytotoxicity of magnetite nanoparticles in Caco-2 cells at concentrations up to 100 μg mL^{-1} [48–50].

The literature also reports that CNTs can interfere with different viability assays. Consequently, more than one test is recommended to ensure the reliability of the results [51]. Resazurin and LDH assays were chosen because they are considered sensible, simple, and fast [52,53]. In addition, their combined results could provide suitable and complementary information regarding cell cytocompatibility and cytotoxicity.

The hemoglobin release rate of M-CNT, M-CNT-BSA, and M-CNT-HL was lower than 1.04 % for all the appraised concentrations (Fig. 4A). This value is significantly lower than the standard reference level (5 %). This indicates that the developed materials do not cause injuries to the RBCs and can be applied *via* intravenous injection.

M-CNT, M-CNT-HL, and M-CNT-BSA were found to be well tolerated by mouse fibroblast cells (L929) (which was selected according to the guidelines of ISO 10993-5 for biocompatibility evaluation) and Caco-2 cells as assessed by the resazurin assay (Fig. 4B and C). The viability of L929 cell line was higher than 70 % [51] for all the tested concentrations. For Caco-2 cells, evidence of a subtle cytotoxic effect was observed only at the highest concentration of M-CNT-HL.

In the LDH assay, the cytotoxic effect was given by the statistical difference between the absorbance values of the control of viability (DMEM) and absorbance of the samples (Fig. 4D and E). Considering the L929 cells, significant differences from the control were observed for concentrations higher than 25 μg mL^{-1} for M-CNT-BSA and higher than 100 μg mL^{-1} for M-CNT and M-CNT-HL. Nevertheless, LDH release was lower than 30 % for concentrations up to 250 μg mL^{-1} for M-CNT and M-CNT-HL and 100 μg mL^{-1} for M-CNT-BSA, demonstrating the limited cytotoxicity of the materials. Considering the Caco-2 cells, significant differences were only observed at concentrations higher than 250 μg mL^{-1} for M-CNT and higher than 400 μg mL^{-1} for M-CNT-HL.

In the LDH assay, the higher cytotoxicity may be related to the cell membrane damage caused by the CNTs [52]. Therefore, the better resistance of Caco-2 cells in the LDH assay may be related to their arrangement in monolayers with tight junctions [53]. The CNTs can interact with the cells by a nanoneedle mechanism, with possibilities of

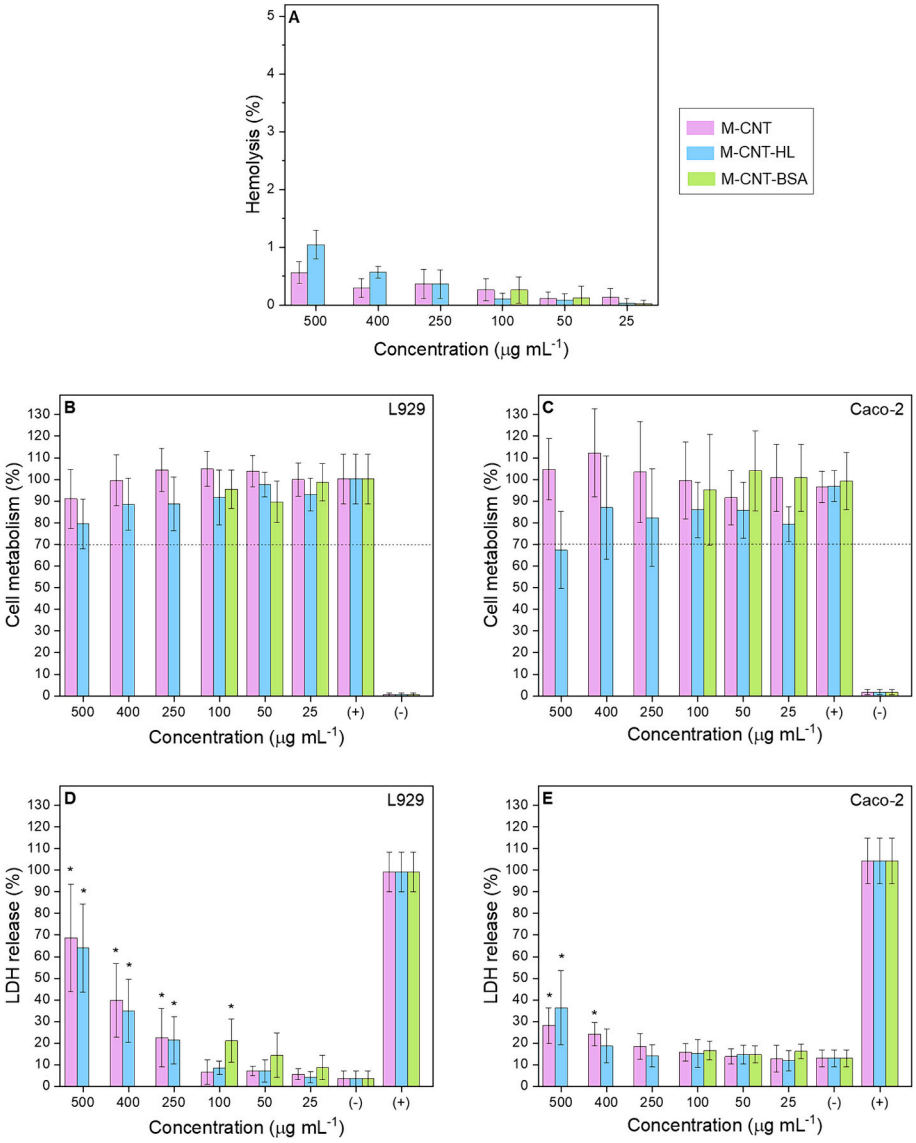

Fig. 4. Hemolysis assay (A). Resazurin and LDH release tests for L929 (B and D) and Caco-2 (C and E) cell lines. Note: The values are represented by mean ± standard deviation ($n > 3$). * denotes statically significant differences ($p < 0.05$) between the concentration and the negative control of each material.

penetration and/or damage (depending on their size, aggregation state, and cell type) [54]. In the performed assays, the nanotubes at the highest concentrations appeared to interact with cells, leading to membrane damage but not necessarily to cell death.

3.3.2. *Generation of reactive oxygen species*

The DCFH-DA probe is enzymatically hydrolyzed to dichlorodihydrofluorescein (DCFH) and, posteriorly, reduced to dichlorofluorescein (DCF) by H_2O_2 species [55]. The DCFH also can be reduced in the presence of Fe^{2+}, with $OH^{\bullet}$ radicals responsible for this reaction [56]. Therefore, DCFH-DA is a good indicator of the generation of intracellular ROS.

Fig. 5 shows the laser-confocal microscopic images of Caco-2 cells treated with M-CNT, M-CNT-BSA, M-CTN-HL (50 μg mL^{-1}), DMEM (negative control), or H_2O_2 solution (positive control). The fluorescence intensity of the probe was estimated from the microscopic images ($n \geq 8$), and the obtained value was divided by the nucleus's fluorescence intensity from the same image. Results of 0.0754, 0.0851, 0.0530, 0.0534, and 0.1710 were obtained for M-CNT, M-CNT-BSA, M-CTN-HL, negative control, and positive control, respectively. These results could indicate that the presence of the nanotubes leads to no increase or a subtle increase in the production of ROS by the cells. ROS generation was also found in the negative control since they are normally produced in the cell's respiratory chain, and cancer cell lines, such as Caco-2, exhibit higher metabolic oxidative stress than normal cells [57].

Additionally, the brightfield images reveal the presence of nanotube aggregates surrounded by cells (Fig. S13). These structures do not appear to harm cells but support their growth. The use of CNTs as scaffolds for tissue reconstruction has been reported in the literature [58,59]. Moreover, it is worth pointing out that the presence of M-CNT-HL aggregates was practically negligible.

The production of ROS determined using the DCFH-DA probe was also quantified by flow cytometry. No statistical difference (Scott-Knott test, 0.05 significance level) was observed between the negative control and the cells treated with M-CNT, M-CNT-BSA, or M-CNT-HL (Fig. 6A). These results corroborate those obtained by the confocal microscopy images, indicating that concentrations equal to or lower than 50 μg mL^{-1} do not increase Caco-2 oxidative stress.

3.3.3. *Apoptosis assay*

The percentage of early and late apoptotic, necrotic, and viable cells was quantified using Annexin V-FITC with the 7-AAD kit. The kit allows

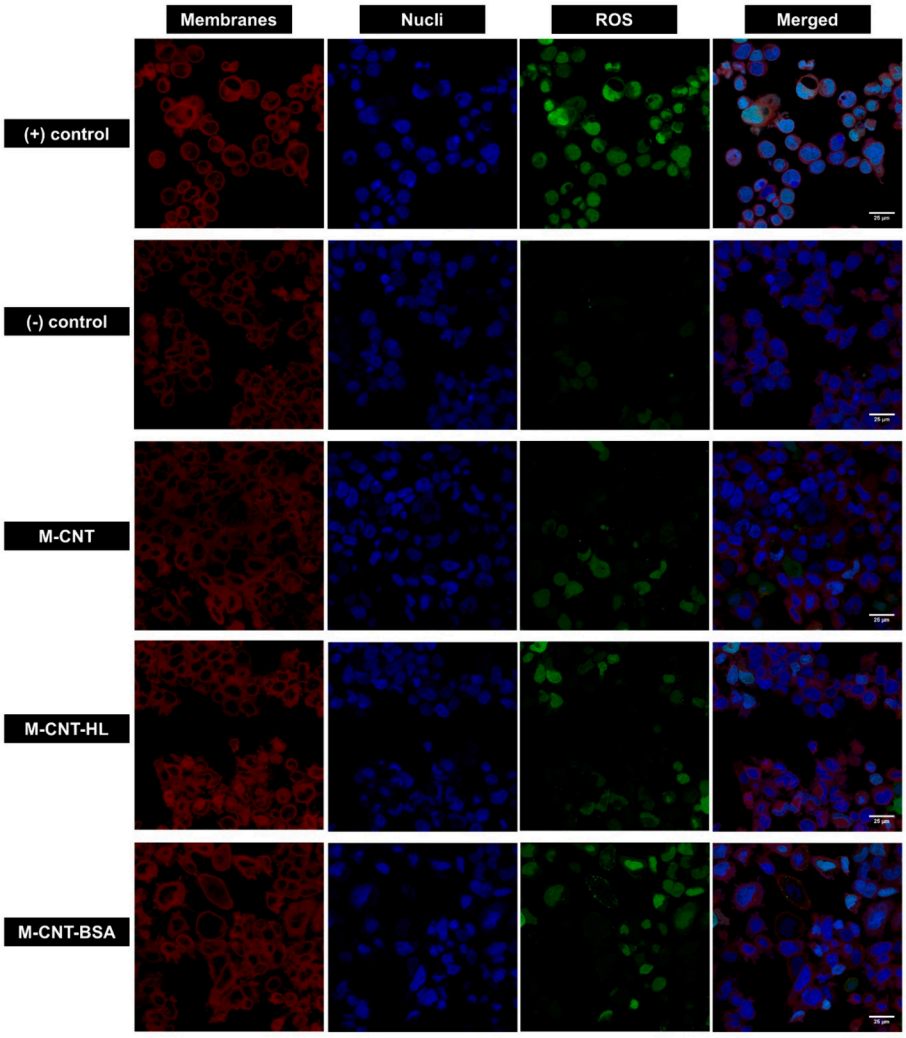

Fig. 5. Laser confocal microscopy from stained Caco-2 cells after the treatment with the synthesized materials and controls: (−) DMEM and (+) H_2O_2 solution. Red channel: Cellmask™ Deep Red. Blue channel: Hoechst 33342®. Green channel: DCFH-DA. Scale: 25 μm. (For interpretation of the references to colour in this figure legend, the reader is referred to the web version of this article.)

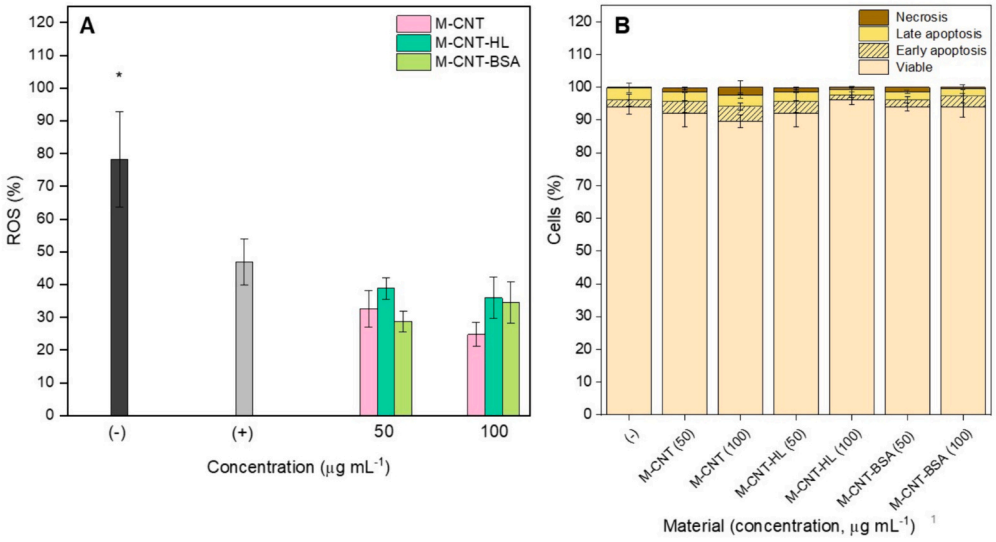

Fig. 6. (A) Oxidative stress of Caco-2 cells. (+) and (−) are the controls using H_2O_2 solution and culture medium, respectively. (B) Percent of viable, apoptotic, and necrotic cells after the treatment with the synthesized materials. (−) control using only culture medium (DMEM).

a study of the translocation of phosphatidylserine to the outer layer of the plasma membrane, which is common in apoptotic stages. On the other hand, only destabilized cells in late apoptosis or necrotic stages are dyed with 7-AAD. Viable cells are not stained [60].

From Fig. 6B, it is possible to see that the percentage of viable cells was not statistically changed ($p > 0.05$) when Caco-2 cells were exposed to M-CNT, M-CNT-BSA, M-CNT-HL suspensions (50 and 100 μg mL^{-1}) or DMEM (negative control). However, the number of necrotic cells increased, principally for M-CNT. When exposed to nanomaterials (50 μg mL^{-1}), necrotic cells increased from 0.1 % (negative control) to 0.8, 0.9, or 1.9 % for M-CNT-BSA, M-CNT-HL, or M-CNT, respectively. The literature corroborates that the chemical surface of nanomaterials plays a role in cell death [61]. Furthermore, carbon materials without surface modifications are hydrophobic and can disrupt cell membranes through hydrophobic interactions, inducing cell apoptosis/necrosis [62] .

The obtained results also show the cytocompatibility of the synthesized materials in concentrations up to 100 μg mL^{-1}, corroborating the previous results of cytotoxicity and production of ROS and suggesting a protective effect conferred by the functionalization groups.

3.4. Caco-2 cells permeability assay

The previous studies point out that concentrations up to 100 μg mL^{-1} of the modified CNTs were cytocompatible and did not cause enhanced oxidative stress in Caco-2 cells. Therefore, 50 μg mL^{-1} was selected as the concentration to proceed with the intestinal permeability assays without compromising the viability of cells and preserving the integrity of the monolayers.

After 21 days of growth, all the seeded Caco-2 monolayers presented TEER values higher than 1000 Ω cm^2 (Fig. S14), and these results were found by others in the literature [63–65]. Considering the transwells that were not exposed to a magnetic field, the TEER values were higher than 200 Ω cm^2 for all the tested samples and time points (1–24 h). This result attested to the integrity of the monolayers throughout the assay [20]. The transwells exposed to the magnets presented TEER values lower than 130 Ω cm^2 at the timepoint of 24 h, both for cells treated with the suspensions of carbon nanotubes or treated with the permeation control (HBSS buffer). After 8 h of exposure, the TEER values were close to 200 Ω cm^2 for cells exposed to the magnets, and longer exposure times would result in damage to the monolayers, impairing the permeation assay. Thus, 8 h was established as the maximum period for studies using transwell devices exposed to the magnetic field. The external magnetic field can increase the concentration and half-life of free radicals by influencing the redox actives' electron pairs [66,67], possibly leading to cell death and monolayer destabilization.

The magnets were placed at the bottom of the transwell plate and used to attract the iron nanoparticles. The literature reports the use of magnetic fields improved the permeation of magnetic materials in models of the blood-brain barrier [68] and epithelial cells [69]. Thus, magnets were used to study this effect in Caco-2 cells. After the permeation assay, the employed CNTs that stayed on the apical side of the non-exposed plates were more easily washed when compared to the exposed plates, which were more tightly attached to the monolayer, indicating the successful action of the magnets.

The quantification of the CNTs in cell permeability assays is uncommon in the literature, with only information regarding the values of TEER being reported [70–73]. In this paper, the iron (presented in the magnetic nanoparticles) was quantified by ICP-MS after the chemical decomposition of the materials, with an estimation of the results of the nanotubes that permeated the Caco-2 monolayers (Fig. 7). From the TGA analyses, it was possible to estimate that 46 % of the synthesized materials were composed of iron nanoparticles. Therefore, this value was used to calculate the masses of the nanotubes that crossed the Caco-2 biomimetic barrier.

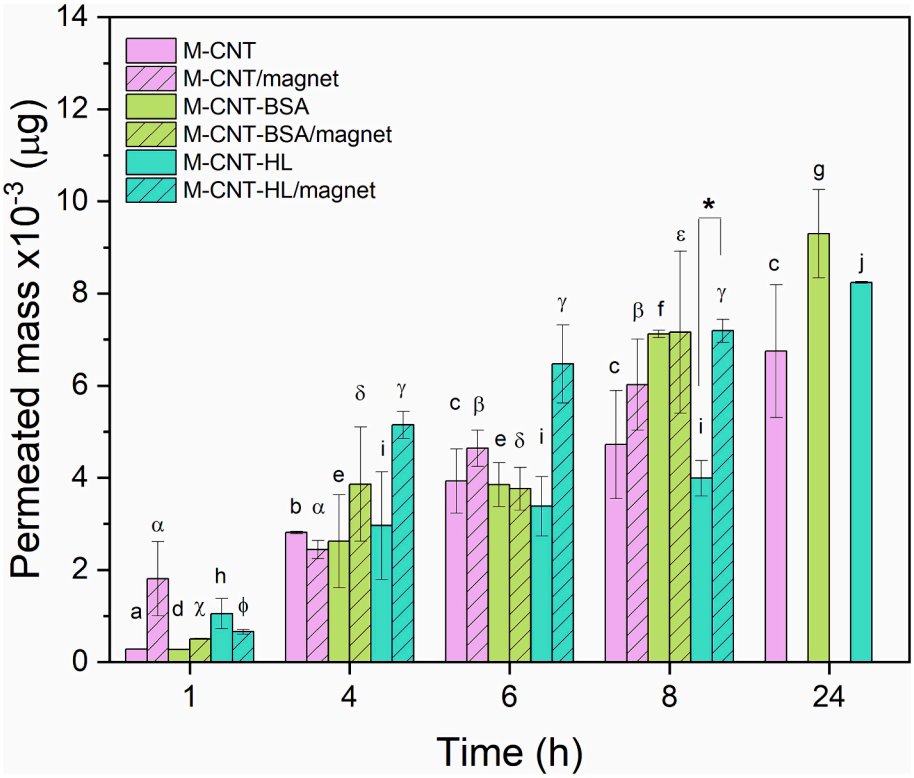

Fig. 7. Permeated mass of magnetic carbon nanotubes (M-CNTs), magnetic carbon nanotubes covered with bovine serum albumin (M-CNTs-BSA), and magnetic carbon nanotubes functionalized with hydrophilic monomers (M-CNTs-HL) exposed and non-exposed to magnets. Note: The data are presented as the mean ± standard deviation ($n = 3$). Equal lowercase or Greek letters indicate equal statistical means for the same treatment. The permeation of samples exposed and not exposed to magnets was compared at the 8 h time point, and * denotes a statistically significant difference ($p < 0.05$).

As can be seen in Fig. 7, there was a tendency for permeation increase over time. After 8 h of cell exposure to the materials, only the M-CNT-HL showed a statistically significant difference in permeation between the monolayers exposed and non-exposed to the magnetic field. Due to its hydrophilicity, M-CNT-HL may have presented some limitations for membrane permeation, which could be overcome by the presence of magnets. Additionally, M-CNT-HL showed better dispersibility in the culture medium. M-CNT achieved maximum permeation capacity, even in the absence of the external magnetic field, probably due to its nanoneedle shape and lack of surface functionalization. The literature reports that the uptake of albumin by Caco-2 is a receptor-mediated process [74,75], which could have contributed to the higher permeation of M-CNT-BSA compared to the other materials when the cells were not exposed to the external magnetic field. However, due to its volume and density, the BSA layer may have hindered the permeation of M-CNT-BSA, and this situation was not improved significantly by exposure to magnets. It is also reported in the literature that the albumin uptake is a saturable process [75]. Finally, even without the statistical difference for M-CNT and M-CNT-BSA regarding the presence of the magnetic field, it was possible to observe a trend towards greater permeation when the monolayers were exposed to the magnets.

Images of the cell's monolayers after 8 or 24 h (for cells exposed and non-exposed to magnets, respectively) were captured using laser confocal microscopy. Fig. 8 represents the 3D images of the biomimetic barrier, demonstrating their sustained integrity despite prolonged nanotube exposure. Furthermore, using Fiji® software, images with a thickness of approximately 30–40 μm were generated, revealing embedded nanotubes. Remarkably, these nanotubes did not appear to inflict damage upon the cell monolayer.

4. Conclusions

All the proposed materials were successfully synthesized, characterized, and evaluated using several *in vitro* assays. The results of cell metabolism and cytotoxicity showed that the studied carbon nanotubes can cause cell membrane damage but do not necessarily lead to cell death. Concentrations up to 100 μg mL^{-1} of all the materials were found to be cytocompatible with both L929 and Caco-2 cells. Assays of ROS and apoptosis induction in Caco-2 cells corroborated these results.

The M-CNT-BSA presented a higher capability to exclude macromolecules, which can be advantageous for further *in vivo* applications; presented a lower tendency to generate ROS, when compared to M-CNT-HL; and had a higher tendency to permeate across the biomimetic membrane, particularly without the use of an external magnetic field. On the other hand, M-CNT-BSA, presented lower stability and dispersibility in the DMEM medium, making impossible the studies of this material at higher applied concentrations (500 and 400 μg mL^{-1}). In contrast, M-CNT-HL presented the most suitable dispersibility in DMEM medium among all the evaluated materials and was the only one that exhibited a statistically significant improvement in the permeation with the use of magnets. Both surface-functionalized nanotubes were effective in preventing the induction of the necrotic process in Caco-2 cells and were favorable to the permeation across the monolayer barrier.

Caco-2 monolayers remained structurally suitable when exposed to an external magnetic field for up to 8 h, as indicated by the TEER measurements. After this period, the magnets caused injuries in the cells, even in the control group. At the end of the permeation assays, stained monolayers were observed under confocal microscopy, showing no significant differences in morphology between the control and the applied treatments. It was demonstrated that the presence of magnetic nanoparticles in the material enables the estimation of materials permeated through the Caco-2 barrier using ICP-MS analysis.

It is noteworthy that some material aggregates were observed by confocal microscopy during different assays; nonetheless, these aggregates did not appear to damage Caco-2 cells and instead served as a scaffold for cell growth. Overall, the obtained data demonstrated that the surface modifications can change the proprieties and the interaction of CNTs with the cells, and provide promising and valuable information, supporting the use of these carbon nanotubes for biomedical applications. Additional experiments with M-CNT, M-CNT-BSA, and M-CNT-HL could be performed to evaluate their suitability for oral drug delivery, such as *in vivo* toxicity, biodistribution, and bioaccumulation studies.

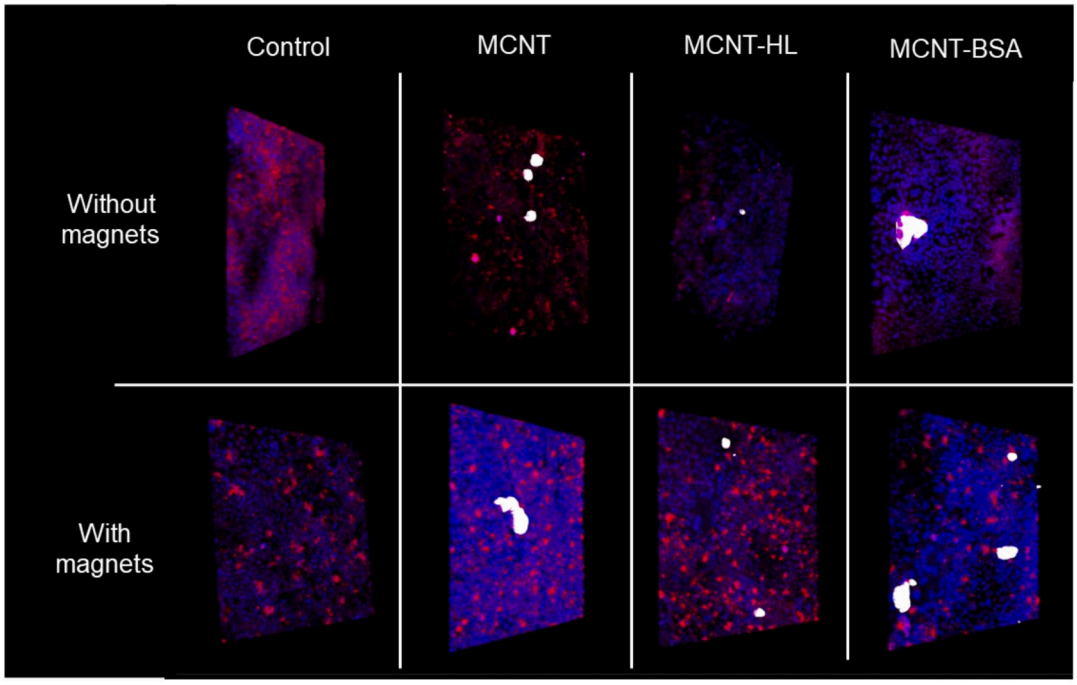

Fig. 8. Caco-2 monolayers after the permeability assay. Membranes and nuclei are dyed in red and blue, respectively. (For interpretation of the references to colour in this figure legend, the reader is referred to the web version of this article.)

CRediT authorship contribution statement

Mariana Azevedo Rosa: Conceptualization, Data curation, Formal analysis, Methodology, Project administration, Validation, Visualisation, Writing – Original Draft. **Andreia Granja:** Formal analysis, Methodology, Validation, Investigation, Writing - Review & Editing. **Cláudia Nunes:** Conceptualization, Formal analysis, Supervision, Writing - Review & Editing. **Salette Reis:** Conceptualization, Funding acquisition, Project administration, Supervision, Writing – Review & Editing. **Ana Beatriz Santos da Silva:** Formal analysis, Methodology. **Ketolly Natanne da Silva Leal:** Methodology, Formal analysis. **Marco Aurélio Zezzi Arruda:** Conceptualization, Funding acquisition, Methoology, Supervision, Writing – Review & Editing. **Luiz Fernando Gorup:** Methodology, Formal analysis, Validation, Writing – Review & Editing. **Mariane Gonçalves Santos:** Conceptualization, Methodology, Writing – Review & Editing. **Marcos Vinicios Salles Dias:** Methodology, Writing – Review & Editing. **Eduardo Costa Figueiredo:** Conceptualization, Data curation, Funding acquisition, Investigation, Methodology, Project administration, Supervision, Validation, Writing – Review & Editing.

Declaration of competing interest

The authors declare the following financial interests/personal relationships which may be considered as potential competing interests: Eduardo Costa Figueiredo reports financial support was provided by Federal University of Alfenas. Mariana Azevedo Rosa reports financial support was provided by Coordination of Higher Education Personnel Improvement. Eduardo Costa Figueiredo reports financial support was provided by Minas Gerais State Foundation of Support to the Research. Eduardo Costa Figueiredo reports financial support was provided by National Council for Scientific and Technological Development. If there are other authors, they declare that they have no known competing financial interests or personal relationships that could have appeared to influence the work reported in this paper.

Acknowledgments

The authors would like to thank the Coordenação de Aperfeiçoamento de Pessoal de Nível Superior (CAPES-Brazil) [Código de Financiamento 001], Conselho Nacional de Desenvolvimento Científico e Tecnológico (CNPq-Brazil) [project 427365/2018-0, 301564/2019-1, 302898/2022-0], and Fundação de Amparo à Pesquisa do Estado de Minas Gerais (FAPEMIG-Brazil) [project APQ-00043-21] for their financial support.

Appendix A. Supplementary data

Supplementary data to this article can be found online at https://doi.org/10.1016/j.ijbiomac.2024.131962.

References

[1] R. Alshehri, A.M. Ilyas, A. Hasan, A. Arnaout, F. Ahmed, A. Memic, Carbon nanotubes in biomedical applications: factors, mechanisms, and remedies of toxicity, J. Med. Chem. 59 (2016) 8149–8167, https://doi.org/10.1021/acs.jmedchem.5b01770.
[2] S.K. Prajapati, A. Jain, C. Shrivastava, A.K. Jain, Hyaluronic acid conjugated multi-walled carbon nanotubes for colon cancer targeting, Int. J. Biol. Macromol. 123 (2019) 691–703, https://doi.org/10.1016/j.ijbiomac.2018.11.116.
[3] C. Paviolo, F.N. Soria, J.S. Ferreira, A. Lee, L. Groc, E. Bezard, L. Cognet, Nanoscale exploration of the extracellular space in the live brain by combining single carbon nanotube tracking and super-resolution imaging analysis, Methods 174 (2020) 91–99, https://doi.org/10.1016/j.ymeth.2019.03.005.
[4] M. Sireesha, V. Jagadeesh Babu, A.S. Kranthi Kiran, S. Ramakrishna, A review on carbon nanotubes in biosensor devices and their applications in medicine, Nanocomposites 4 (2018) 36–57, https://doi.org/10.1080/20550324.2018.1478765.
[5] B.K. Shrestha, S. Shrestha, A.P. Tiwari, J.-I. Kim, S.W. Ko, H.-J. Kim, C.H. Park, C. S. Kim, Bio-inspired hybrid scaffold of zinc oxide-functionalized multi-wall carbon nanotubes reinforced polyurethane nanofibers for bone tissue engineering, Mater. Des. 133 (2017) 69–81, https://doi.org/10.1016/j.matdes.2017.07.049.
[6] N. Belali, N. Wathoni, M. Muchtaridi, Advances in orally targeted drug delivery to colon, J. Adv. Pharm. Technol. Res. 10 (2019) 100–106, https://doi.org/10.4103/japtr.JAPTR_26_19.
[7] D. Gonzalez-Carter, A.E. Goode, D. Kiryushko, S. Masuda, S. Hu, R. Lopes-Rodrigues, D.T. Dexter, M.S.P. Shaffer, A.E. Porter, Quantification of blood-brain barrier transport and neuronal toxicity of unlabelled multiwalled carbon nanotubes as a function of surface charge, Nanoscale 11 (2019) 22054–22069, https://doi.org/10.1039/c9nr02866h.
[8] J. Simon, E. Flahaut, M. Golzio, Overview of carbon nanotubes for biomedical applications, Materials 12 (2019) 1–21, https://doi.org/10.3390/ma12040624.
[9] S.K. Prajapati, A. Malaiya, P. Kesharwani, D. Soni, A. Jain, Biomedical applications and toxicities of carbon nanotubes, Drug Chem. Toxicol. 45 (2022) 435–450, https://doi.org/10.1080/01480545.2019.1709492.
[10] G. Fotakis, J.A. Timbrell, In vitro cytotoxicity assays: comparison of LDH, neutral red, MTT and protein assay in hepatoma cell lines following exposure to cadmium chloride, Toxicol. Lett. 160 (2006) 171–177, https://doi.org/10.1016/j.toxlet.2005.07.001.
[11] J. Long, X. Li, Y. Kang, Y. Ding, Z. Gu, Y. Cao, Internalization, cytotoxicity, oxidative stress and inflammation of multi-walled carbon nanotubes in human endothelial cells: influence of pre-incubation with bovine serum albumin, RSC Adv. 8 (2018) 9253–9260, https://doi.org/10.1039/C8RA00445E.
[12] N. Lu, Y. Sui, R. Tian, Y.-Y. Peng, Adsorption of plasma proteins on single-walled carbon nanotubes reduced cytotoxicity and modulated neutrophil activation, Chem. Res. Toxicol. 31 (2018) 1061–1068, https://doi.org/10.1021/acs.chemrestox.8b00141.
[13] Y. Ding, R. Tian, Z. Yang, J. Chen, N. Lu, Effects of serum albumin on the degradation and cytotoxicity of single-walled carbon nanotubes, Biophys. Chem. 222 (2017) 1–6, https://doi.org/10.1016/j.bpc.2016.12.002.
[14] L. Zhou, H.J. Forman, Y. Ge, J. Lunec, Multi-walled carbon nanotubes: a cytotoxicity study in relation to functionalization, dose and dispersion, Toxicol. In Vitro 42 (2017) 292–298, https://doi.org/10.1016/j.tiv.2017.04.027.
[15] B. Kaboudin, F. Saghatchi, F. Kazemi, S. Akbari-Birgani, A novel magnetic carbon nanotubes functionalized with pyridine groups: synthesis, characterization and their application as an efficient carrier for plasmid DNA and aptamer, ChemistrySelect 3 (2018) 6743–6749, https://doi.org/10.1002/slct.201800708.
[16] L. Xu, L. Feng, S. Dong, J. Hao, Q. Yu, Carbon nanotubes modified by a paramagnetic cationic surfactant for migration of DNA and proteins, Colloids Surf. A Physicochem. Eng. Asp. 559 (2018) 201–208, https://doi.org/10.1016/j.colsurfa.2018.09.032.
[17] Q. Hu, Y. Bu, R. Cao, G. Zhang, X. Xie, S. Wang, Stability designs of cell membrane cloaked magnetic carbon nanotubes for improved life span in screening drug leads, Anal. Chem. 91 (2019) 13062–13070, https://doi.org/10.1021/acs.analchem.9b03268.
[18] K. Kostarelos, L. Lacerda, G. Pastorin, W. Wu, S. Wieckowski, J. Luangsivilay, S. Godefroy, D. Pantarotto, J.-P. Briand, S. Muller, M. Prato, A. Bianco, Cellular uptake of functionalized carbon nanotubes is independent of functional group and cell type, Nat. Nanotechnol. 2 (2007) 108–113, https://doi.org/10.1038/nnano.2006.209.
[19] Y. Sambuy, I. De Angelis, G. Ranaldi, M.L. Scarino, A. Stammati, F. Zucco, The Caco-2 cell line as a model of the intestinal barrier: influence of cell and culture-related factors on Caco-2 cell functional characteristics, Cell Biol. Toxicol. 21 (2005) 1–26, https://doi.org/10.1007/s10565-005-0085-6.
[20] A. Granja, A.R. Neves, C.T. Sousa, M. Pinheiro, S. Reis, EGCG intestinal absorption and oral bioavailability enhancement using folic acid-functionalized nanostructured lipid carriers, Heliyon 5 (2019) e02020, https://doi.org/10.1016/j.heliyon.2019.e02020.
[21] V. Pade, S. Stavchansky, Link between drug absorption solubility and permeability measurements in Caco-2 cells, J. Pharm. Sci. 87 (1998) 1604–1607, https://doi.org/10.1021/js980111k.
[22] J. Kolosnjaj-Tabi, K.B. Hartman, S. Boudjemaa, J.S. Ananta, G. Morgant, H. Szwarc, L.J. Wilson, F. Moussa, In vivo behavior of large doses of ultrashort and full-length single-walled carbon nanotubes after oral and intraperitoneal administration to Swiss mice, ACS Nano 4 (2010) 1481–1492, https://doi.org/10.1021/nn901573w.
[23] V.K. Prajapati, K. Awasthi, T.P. Yadav, M. Rai, O.N. Srivastava, S. Sundar, An oral formulation of amphotericin B attached to functionalized carbon nanotubes is an effective treatment for experimental visceral leishmaniasis, J. Infect. Dis. 205 (2012) 333–336, https://doi.org/10.1093/infdis/jir735.
[24] H. Chen, R. Zhao, B. Wang, L. Zheng, H. Ouyang, H. Wang, X. Zhou, D. Zhang, Z. Chai, Y. Zhao, W. Feng, Acute Oral administration of single-walled carbon nanotubes increases intestinal permeability and inflammatory responses: association with the changes in gut microbiota in mice, Adv. Healthc. Mater. 7 (2018) 1701313, https://doi.org/10.1002/adhm.201701313.
[25] C. Espíndola, A.J. Correa, M. López-López, P. López-Cornejo, E. Bernal, J. A. Lebrón, F.J. Ostos, M.R.E.I. Benhnia, M.L. Moyá, Single -and multi-walled carbon nanotubes as nanocarriers for the delivery of 7-hydroxyflavone, Pharmaceutics 14 (2022), https://doi.org/10.3390/pharmaceutics14122806.
[26] J.C. Cruz, M.A. Rosa, L. Morés, E. Carasek, J.A. de S. Crippa, E.C. Figueiredo, M.E. C. Queiroz, Magnetic restricted-access carbon nanotubes for SPME to determine cannabinoids in plasma samples by UHPLC-MS/MS, Anal. Chim. Acta 1226 (2022) 3–12, https://doi.org/10.1016/j.aca.2022.340160.
[27] S. Lin, C. Zou, H. Liang, H. Peng, Y. Liao, The effective removal of nickel ions from aqueous solution onto magnetic multi-walled carbon nanotubes modified by β-cyclodextrin, Colloids Surf. A Physicochem. Eng. Asp. 619 (2021) 126544, https://doi.org/10.1016/j.colsurfa.2021.126544.

[28] T.V. Mendes, L.S. Franqui, M.G. Santos, C. Wisniewski, E.C. Figueiredo, Synthesis and characterization of a new magnetic restricted access molecularly imprinted polymer for biological sample preparation, Mater. Today Commun. 24 (2020) 101002, https://doi.org/10.1016/j.mtcomm.2020.101002.
[29] H.D. de Faria, A.T. Silveira, B.C. do Prado, J.L.M. Nacif, M.A. Rosa, J. da R. dos Santos, P.C.J.L. Santos, E.C. Figueiredo, I. Martins, Online biological sample preparation with restricted access hybrid carbon nanotubes for determination of anti-smoking drugs, J. Chromatogr. A 1669 (2022) 462931, https://doi.org/10.1016/j.chroma.2022.462931.
[30] A. Granja, R. Lima-Sousa, C.G. Alves, D. de Melo-Diogo, M. Pinheiro, C.T. Sousa, I. J. Correia, S. Reis, Mitoxantrone-loaded lipid nanoparticles for breast cancer therapy – quality-by-design approach and efficacy assessment in 2D and 3D in vitro cancer models, Int. J. Pharm. 607 (2021) 121044, https://doi.org/10.1016/j.ijpharm.2021.121044.
[31] J.R. de Jesus, A.Z.B. Aragão, M.A.Z. Arruda, C.H.I. Ramos, Optimization of a methodology for quantification and removal of zinc gives insights into the effect of this metal on the stability and function of the zinc-binding Co-chaperone Ydj1, Front. Chem. 7 (2019), https://doi.org/10.3389/fchem.2019.00416.
[32] M.L. Menezes, G. Fèlix, On line extraction and separation of bendiocarb, methomyl, methylparathion, and pentachlorophenol pesticides from raw milk, J. Liq. Chromatogr. Relat. Technol. 21 (1998) 2863–2871, https://doi.org/10.1080/10826079808003449.
[33] H.D. de Faria, M.A. Rosa, A.T. Silveira, E.C. Figueiredo, Direct extraction of tetracyclines from bovine milk using restricted access carbon nanotubes in a column switching liquid chromatography system, Food Chem. 225 (2017) 98–106, https://doi.org/10.1016/j.foodchem.2017.01.004.
[34] H.D. de Faria, L.C. de C. Abrão, M.G. Santos, A.F. Barbosa, E.C. Figueiredo, New advances in restricted access materials for sample preparation: a review, Anal. Chim. Acta (2017), https://doi.org/10.1016/j.aca.2016.12.047.
[35] A.F. Barbosa, V.M.P. Barbosa, J. Bettini, P.O. Luccas, E.C. Figueiredo, Restricted access carbon nanotubes for direct extraction of cadmium from human serum samples followed by atomic absorption spectrometry analysis, Talanta 131 (2015) 213–220, https://doi.org/10.1016/j.talanta.2014.07.051.
[36] T. Al Mgheer, F.H. Abdulrazzak, Oxidation of multi-walled carbon nanotubes in acidic and basic piranha mixture, Front. Nanosci. Nanotechnol. 2 (2016), https://doi.org/10.15761/FNN.1000127.
[37] A. Tadjarodi, M. Haghverdi, V. Mohammadi, Preparation and characterization of nano-porous silica aerogel from rice husk ash by drying at atmospheric pressure, Mater. Res. Bull. 47 (2012) 2584–2589, https://doi.org/10.1016/j.materresbull.2012.04.143.
[38] S.M. Fakhrhoseini, Q. Li, V. Unnikrishnan, M. Naebe, Nano-magnetite decorated carbon fibre for enhanced interfacial shear strength, Carbon N Y 148 (2019) 361–369, https://doi.org/10.1016/j.carbon.2019.03.078.
[39] T. Zhao, C. Hou, H. Zhang, R. Zhu, S. She, J. Wang, T. Li, Z. Liu, B. Wei, Electromagnetic wave absorbing properties of amorphous carbon nanotubes, Sci. Rep. 4 (2015) 5619, https://doi.org/10.1038/srep05619.
[40] L. Nalbandian, A. Delimitis, V.T. Zaspalis, E.A. Deliyanni, D.N. Bakoyannakis, E. N. Peleka, Hydrothermally prepared nanocrystalline Mn-Zn ferrites: synthesis and characterization, Microporous Mesoporous Mater. 114 (2008) 465–473, https://doi.org/10.1016/j.micromeso.2008.01.034.
[41] F. Mohammad Aminzadeh, B. Zeynizadeh, Immobilized nickel boride nanoparticles on magnetic functionalized multi-walled carbon nanotubes: a new nanocomposite for the efficient one-pot synthesis of 1,4-benzodiazepines, Nanoscale Adv. 5 (2023) 4499–4520, https://doi.org/10.1039/D3NA00415E.
[42] A.C. do Lago, M.H. da Silva Cavalcanti, M.A. Rosa, A.T. Silveira, C.R. Teixeira Tarley, E.C. Figueiredo, Magnetic restricted-access carbon nanotubes for dispersive solid phase extraction of organophosphates pesticides from bovine milk samples, Anal. Chim. Acta 1102 (2020) 11–23, https://doi.org/10.1016/j.aca.2019.12.039.
[43] X. Zeng, S. Yu, L. Ye, M. Li, Z. Pan, R. Sun, J. Xu, Encapsulating carbon nanotubes with SiO2: A strategy for applying them in polymer nanocomposites with high mechanical strength and electrical insulation, J. Mater. Chem. C Mater. 3 (2015) 187–195, https://doi.org/10.1039/C4TC01051E.
[44] P.P. Bergmann CP, Raman spectroscopy of iron oxide of nanoparticles (Fe3O4), J. Mater. Sci. Eng. 05 (2015), https://doi.org/10.4172/2169-0022.1000217.
[45] Y.-X. Wang, J.L. Robertson, W.B. Spillman Jr., R.O. Claus, Effects of the chemical structure and the surface properties of polymeric biomaterials on their biocompatibility, Pharm. Res. 21 (2004) 1362–1373, https://doi.org/10.1023/B:PHAM.0000036909.41843.18.
[46] D. Maiolo, P. Del Pino, P. Metrangolo, W.J. Parak, F. Baldelli Bombelli, Nanomedicine delivery: does protein corona route to the target or off road? Nanomedicine 10 (2015) 3231–3247, https://doi.org/10.2217/nnm.15.163.
[47] S. Tenzer, D. Docter, J. Kuharev, A. Musyanovych, V. Fetz, R. Hecht, F. Schlenk, D. Fischer, K. Kiouptsi, C. Reinhardt, K. Landfester, H. Schild, M. Maskos, S. K. Knauer, R.H. Stauber, Rapid formation of plasma protein corona critically affects nanoparticle pathophysiology, Nat. Nanotechnol. 8 (2013) 772–781, https://doi.org/10.1038/nnano.2013.181.
[48] H. Hildebrand, D. Kühnel, A. Potthoff, K. Mackenzie, A. Springer, K. Schirmer, Evaluating the cytotoxicity of palladium/magnetite nano-catalysts intended for wastewater treatment, Environ. Pollut. 158 (2010) 65–73, https://doi.org/10.1016/j.envpol.2009.08.021.
[49] S. Genc, A. Taghizadehghalehjoughi, Y. Yeni, A. Jafarizad, A. Hacimuftuoglu, D. Nikitovic, A.O. Docea, Y. Mezhuev, A. Tsatsakis, Fe3O4 nanoparticles in combination with 5-FU exert antitumor effects superior to those of the active drug in a colon cancer cell model, Pharmaceutics 15 (2023) 245, https://doi.org/10.3390/pharmaceutics15010245.
[50] A. Ivask, T. Titma, M. Visnapuu, H. Vija, A. Kakinen, M. Sihtmae, S. Pokhrel, L. Madler, M. Heinlaan, V. Kisand, R. Shimmo, A. Kahru, Toxicity of 11 metal oxide nanoparticles to three mammalian cell types in vitro, Curr. Top. Med. Chem. 15 (2015) 1914–1929, https://doi.org/10.2174/1568026615666150506150109.
[51] ISO 10993-5, Biological evaluation of medical devices — Part 5: Tests for in vitro cytotoxicity, 2009.
[52] W. Jiang, Q. Wang, X. Qu, L. Wang, X. Wei, D. Zhu, K. Yang, Effects of charge and surface defects of multi-walled carbon nanotubes on the disruption of model cell membranes, Sci. Total Environ. 574 (2017) 771–780, https://doi.org/10.1016/j.scitotenv.2016.09.150.
[53] D. Ye, M. Bramini, D.R. Hristov, S. Wan, A. Salvati, C. Åberg, K.A. Dawson, Low uptake of silica nanoparticles in Caco-2 intestinal epithelial barriers, Beilstein J. Nanotechnol. 8 (2017) 1396–1406, https://doi.org/10.3762/bjnano.8.141.
[54] C.J. Serpell, K. Kostarelos, B.G. Davis, Can carbon nanotubes deliver on their promise in biology? Harnessing unique properties for unparalleled applications, ACS Cent. Sci. 2 (2016) 190–200, https://doi.org/10.1021/acscentsci.6b00005.
[55] A. Gomes, E. Fernandes, J.L.F.C. Lima, Fluorescence probes used for detection of reactive oxygen species, J. Biochem. Biophys. Methods 65 (2005) 45–80, https://doi.org/10.1016/j.jbbm.2005.10.003.
[56] S. Walrand, S. Valeix, C. Rodriguez, P. Ligot, J. Chassagne, M.-P. Vasson, Flow cytometry study of polymorphonuclear neutrophil oxidative burst: a comparison of three fluorescent probes, Clin. Chim. Acta 331 (2003) 103–110, https://doi.org/10.1016/S0009-8981(03)00086-X.
[57] S. Kumari, A.K. Badana, M.M. G, S. G, R. Malla, Reactive oxygen species: a key constituent in cancer survival, Biomark. Insights 13 (2018) 117727191875539, https://doi.org/10.1177/1177271918755391.
[58] M. Nikbakht, S. Karbasi, S.M. Rezayat, S. Tavakol, E. Sharifi, Evaluation of the effects of hyaluronic acid on poly (3-hydroxybutyrate)/chitosan/carbon nanotubes electrospun scaffold: structure and mechanical properties, Polymer-Plastics Technology and Materials 58 (2019) 2031–2040, https://doi.org/10.1080/25740881.2019.1602645.
[59] P. Zadehnajar, B. Akbari, S. Karbasi, M.H. Mirmusavi, Preparation and characterization of poly ε -caprolactone-gelatin/multi-walled carbon nanotubes electrospun scaffolds for cartilage tissue engineering applications, Int. J. Polymeric Mater. Polymeric Biomater. 69 (2020) 326–337, https://doi.org/10.1080/00914037.2018.1563088.
[60] A.J. Coutinho, S.A. Costa Lima, C.M.M. Afonso, S. Reis, Mucoadhesive and pH responsive fucoidan-chitosan nanoparticles for the oral delivery of methotrexate, Int. J. Biol. Macromol. 158 (2020) 180–188, https://doi.org/10.1016/j.ijbiomac.2020.04.233.
[61] D. De Stefano, R. Carnuccio, M.C. Maiuri, Nanomaterials toxicity and cell death modalities, J. Drug Deliv. 2012 (2012) 1–14, https://doi.org/10.1155/2012/167896.
[62] F. Tian, D. Cui, H. Schwarz, G.G. Estrada, H. Kobayashi, Cytotoxicity of single-wall carbon nanotubes on human fibroblasts, Toxicol. In Vitro 20 (2006) 1202–1212, https://doi.org/10.1016/j.tiv.2006.03.008.
[63] M. Netzel, G. Netzel, D. Zabaras, L. Lundin, L. Day, R. Addepalli, S.A. Osborne, R. Seymour, Release and absorption of carotenes from processed carrots (Daucus carota) using in vitro digestion coupled with a Caco-2 cell trans-well culture model, Food Res. Int. 44 (2011) 868–874, https://doi.org/10.1016/j.foodres.2010.10.058.
[64] R. Zhang, Q. Zhang, L.Q. Ma, X. Cui, Effects of food constituents on absorption and bioaccessibility of dietary synthetic phenolic antioxidant by Caco-2 cells, J. Agric. Food Chem. 68 (2020) 4670–4677, https://doi.org/10.1021/acs.jafc.9b07315.
[65] N.J. Darling, C.L. Mobbs, A.L. González-Hau, M. Freer, S. Przyborski, Bioengineering novel in vitro co-culture models that represent the human intestinal mucosa with improved Caco-2 structure and barrier function, Front. Bioeng. Biotechnol. 8 (2020), https://doi.org/10.3389/fbioe.2020.00992.
[66] S. Ghodbane, A. Lahbib, M. Sakly, H. Abdelmelek, Bioeffects of static magnetic fields: oxidative stress, genotoxic effects, and cancer studies, Biomed. Res. Int. 2013 (2013) 1–12, https://doi.org/10.1155/2013/602987.
[67] M.A. Sharpe, D.S. Baskin, K. Pichumani, O.B. Ijare, S.A. Helekar, Rotating magnetic fields inhibit mitochondrial respiration, promote oxidative stress and produce loss of mitochondrial integrity in cancer cells, Front. Oncol. 11 (2021), https://doi.org/10.3389/fonc.2021.768758.
[68] Saiyed Nair, Gandhi, Magnetic nanoformulation of azidothymidine 5′-triphosphate for targeted delivery across the blood-brain barrier, Int. J. Nanomedicine (2010) 157, https://doi.org/10.2147/IJN.S8905.
[69] K.A. Min, F. Yu, V.C. Yang, X. Zhang, G.R. Rosania, Transcellular transport of heparin-coated magnetic iron oxide nanoparticles (Hep-MION) under the influence of an applied magnetic field, Pharmaceutics 2 (2010) 119–135, https://doi.org/10.3390/pharmaceutics2020119.
[70] M. Pacurari, Y. Qian, W. Fu, D. Schwegler-Berry, M. Ding, V. Castranova, N.L. Guo, Cell permeability, migration, and reactive oxygen species induced by multiwalled carbon nanotubes in human microvascular endothelial cells, J. Toxicol. Environ. Health A 75 (2012) 112–128, https://doi.org/10.1080/15287394.2011.615110.
[71] B.M. Rotoli, O. Bussolati, M.G. Bianchi, A. Barilli, C. Balasubramanian, S. Bellucci, E. Bergamaschi, Non-functionalized multi-walled carbon nanotubes alter the paracellular permeability of human airway epithelial cells, Toxicol. Lett. 178 (2008) 95–102, https://doi.org/10.1016/j.toxlet.2008.02.007.
[72] D. Yang, J. Shen, J. Fan, Y. Chen, X. Guo, Paracellular permeability changes induced by multi-walled carbon nanotubes in brain endothelial cells and associated roles of hemichannels, Toxicology 440 (2020) 152491, https://doi.org/10.1016/j.tox.2020.152491.

[73] A.P. Singh, Md.B. Mia, R.K. Saxena, Acid-functionalized single-walled carbon nanotubes alter epithelial tight junctions and enhance paracellular permeability, J. Biosci. 45 (2020) 23, https://doi.org/10.1007/s12038-020-9989-9.
[74] C. Azevedo, J. Nilsen, A. Grevys, R. Nunes, J.T. Andersen, B. Sarmento, Engineered albumin-functionalized nanoparticles for improved FcRn binding enhance oral delivery of insulin, J. Control. Release 327 (2020) 161–173, https://doi.org/10.1016/j.jconrel.2020.08.005.
[75] L. Hashem, M. Swedrowska, D. Vllasaliu, Intestinal uptake and transport of albumin nanoparticles: potential for oral delivery, Nanomedicine 13 (2018) 1255–1265, https://doi.org/10.2217/nnm-2018-0029.